Available online at www.sciencedirect.com

jmr&t Journal of Materials Research and Technology

https://www.journals.elsevier.com/journal-of-materials-research-and-technology

Original Article

The formation mechanism of the lamellar phase precipitated during solid solution treatment in the Mg-Gd-Al alloy

Yongpeng Zhuang[a], Pengwen Zhou[c], Hongxia Wang[a,b,*], Kaibo Nie[a], Yiming Liu[a], Wei Liang[a,b], Lifei Wang[a], Liuwei Zheng[a,*]

[a] Shanxi Key Laboratory of Advanced Magnesium based Materials, College of Materials Science and Engineering, Taiyuan University of Technology, Taiyuan 030024, China

[b] Key Laboratory of Interface Science and Engineering in Advanced Materials, Taiyuan University of Technology, Ministry of Education, Taiyuan Shanxi 030024, China

[c] Shanxi Aerospace Qinghua Equipment Co., Ltd., Changzhi 046012, China

ARTICLE INFO

Article history:
Received 1 July 2020
Accepted 5 August 2020
Available online 25 August 2020

Keywords:
Lamellar phase
Mg-Gd-Al alloy
Solution treatment
Second phase strengthening

ABSTRACT

A large amount of lamellar phases were precipitated in Mg-9Gd-xAl (x = 0.4, 0.6, 0.8, 1.0, 3.0 wt.%) alloy after solution treatment. In order to explore the composition and formation condition of the lamellar phase, the Mg-9Gd-xAl alloys were subjected to solution treatment at different time, then the influence of lamellar phase on mechanical properties was investigated in Mg-9Gd-xAl alloys. The results indicate that the lamellar phase consists of three elements, Mg, Al, and Gd, and the atomic ratio is close to 1:1:1. It was identified that the lamellar phase is $(Mg, Al)_2Gd$ phase which has the same crystal structure with Al_2Gd. In addition, the lamellar phases were parallel to each other inside one grain, but the alignment directions inside the adjacent grains were different, which provide strong second phase strengthening effect. After solution treatment, the ultimate tensile strength of Mg-9Gd-0.6Al alloy with abundant lamellar phase is greatly improved to 193 MPa.

1. Introduction

Magnesium alloy is widely used in automobile and aerospace industry because of its low density, high specific strength and remarkable casting performance [1–5]. The rare earth element has been an active research topic due to its improvement effect to the strength and high temperature performance of the magnesium alloy [6–9]. Specially, the Gd element has attracted more attention attributed to its relatively high solid solubility and grain refining effect [10–12]. It has been found that the yield strength of Mg alloy (T4) increase 3.3 times after adding 9.26 wt.% Gd [13]. To further enhance the comprehensive performance of Mg alloys containing rare-earth, the non-rare earth element Al was added. Previous studies have shown that the addition of Al can not only refine the grains, but also control the microstructure of the alloy, resulting in fine grain strengthening and second phase strengthening [14–16].

* Corresponding authors.
E-mails: wanghxia1217@163.com (H. Wang), zhengliuwei@tyut.edu.cn (L. Zheng).

https://doi.org/10.1016/j.jmrt.2020.08.024

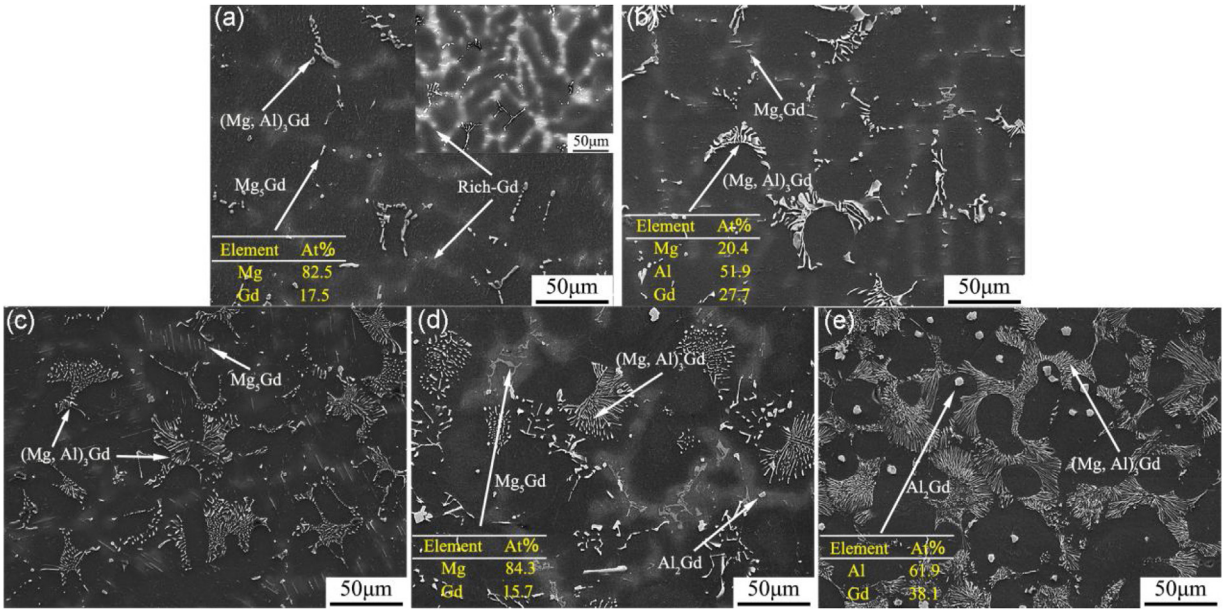

Fig. 1 – SEM-EDS/BSE images of as-cast Mg-9Gd alloys with various Al addition: (a) 0.4 wt.%, (b) 0.6 wt.%, (c) 0.8 wt.%, (d) 1.0 wt.%, (e) 3.0 wt.%.

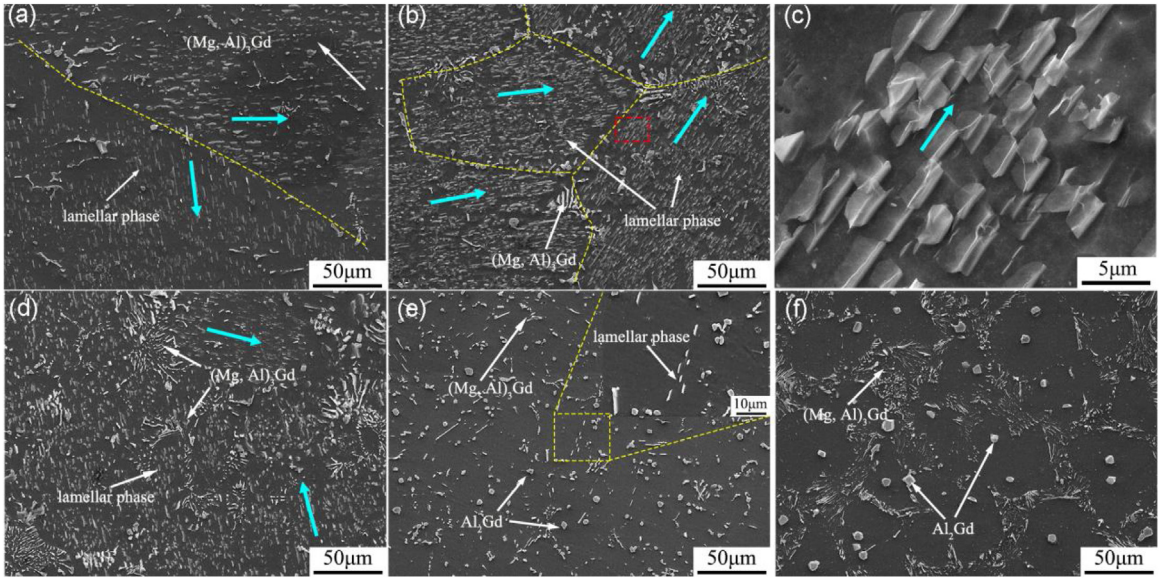

Fig. 2 – SEM micrographs of solid solution treated (20 h) Mg-9Gd-xAl alloys: (a) 0.4 wt.%, (b) 0.6 wt.%, (c) magnified SEM micrograph of red square frame in (b), (d) 0.8 wt.%, (e) 1.0 wt.%, (f) 3.0 wt.%.

There are mainly two intermetallic compounds formed in Mg-Gd alloy by adding Al element, which named Al_2Gd and $(Mg, Al)_3Gd$ phase. Among them, the bulk Al_2Gd has a higher melting point (1798 K) and its particle size increases as the Al content increases [17,18]. The $(Mg, Al)_3Gd$ phase with melting point of 823 K formed as a continuous network structure with the increase of Al content [19]. They both have adverse effects on the properties due to their isolation effects on the matrix. Typically, the solution treatment is applied to eliminate the adverse effect through dissolving the phases into the matrix before deformation or aging treatment. It has been reported that the coarse Mg-Al-Gd phase and the Mg_5Gd phase disappear substantially when the Mg-10Gd-1Al (wt.%) alloy was solution treated at 823 K. At the same time, a new lamellar phase is formed inside the grains, and the essence of the lamellar phase is considered to be Al_2Gd phase [20]. Kishida et al. [21,22] found that a lamellar phase was formed at the grain boundary when the Mg-5.0Gd-3.5Al (at.%) alloy was solution-treated at 798 K, which was presumed as a kind of long-period phase. Gu et al. [23,24] found lamellar phase in $Mg_{97}Al_1Gd_2$ (at.%) alloy after solution treatment at 793 K for 2 h. It is speculated that the crystal structure of the lamellar phase is a face-centered cubic (fcc) structure. Obviously, there is much controversy about the study of the structure

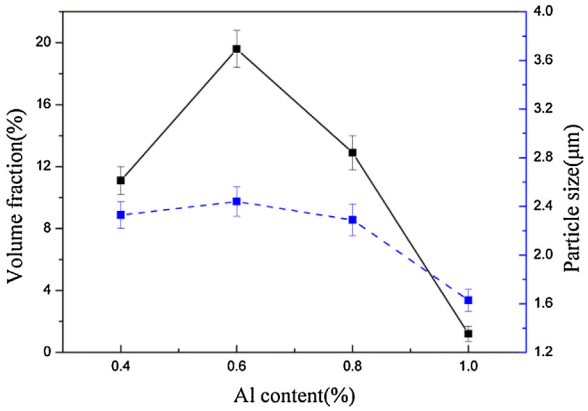

Fig. 3 – The lamellar phase size and volume fraction of Mg-9Gd-xAl alloys after solution treatment by 20 h.

of the lamellar phase. In addition, there is little research on the microstructure evolution of the lamellar phase with the solid solution time and the effect of lamellar phase on the properties of the Mg-Gd-Al alloys.

Hence, in this study, the Mg-Gd alloys with different Al content were treated by solution treatment under different times. The evolution of the lamellar phase and the effect of the lamellar phase on the mechanical properties of alloy were investigated systematically. In addition, the formation mechanism of the lamellar phase was detailed discussed.

2. Experimental procedure

The Mg-9Gd-xAl ($x = 0.4, 0.6, 0.8, 1.0, 3.0$ wt.%) alloys were made from pure Mg (99.99 wt.%), pure Al (99.99 wt.%) and Mg-30Gd (wt.%) master alloy in an electric furnace protected by the mixed protective gas consisting of CO_2 and SF_6. Pure Al and appropriate amounts of pure Mg were added into a steel crucible which was preheated at 673 K, then the temperature was raised to 993 K and held for 20 min. After being stirred for 2 min, Mg-30Gd master alloy was mixed to the melt, which was held at 1023 K for 30 min to make Mg, Gd and Al react completely, and finally poured into steel molds with a diameter of 75 mm, which was preheated to 523 K. Then, the samples were solution treated at 803 K for a series of times followed by water quench. Tensile tests were conducted on a DNSl00 test machine with a speed of 0.5 mm/min. And the Vickers hardness test performed on HVS1000A.

Samples for scanning electron microscopy (SEM, TESCAN Mira3 LMH) were polished and etched in the solution consisted by 4 ml nitric acid and 96 ml ethyl alcohol. The second phase identities were determined by energy dispersive X-ray spectroscopy (EDS) and an X-ray diffractometer (XRD) using TD-3500 equipped with a Cu anode at a scanning velocity of 6°/min and range of 20–80°. The transmission electron microscopy (TEM) using a JEM-2100F (JEOL Ltd, Tokyo, Japan) was applied to certified the crystal structure of second phases. The samples for TEM analysis were prepared by Gatan691 ion milling. The sample speed is 4 rpm, the ion beam voltage is 5 keV, and the angle of ion gun is ±10°.

3. Results and discussion

Fig. 1 shows the SEM-EDS/BSE images of as-cast Mg-9Gd-xAl alloys. It can be observed in Fig. 1(a), the enrichment Gd element regions regarded as white regions in SEM images appear in the Mg-9Gd alloy when the Al contents are less than 1.0 wt.%, but disappear in Mg-9Gd-3Al alloy. As observed in Fig. 1(a)–(d), the short rod-like Mg_5Gd phase distributes in the white regions in Mg-9Gd-0.4Al alloy and increases gradually, finally transforms to net-like when the Al content reaches to 1.0 wt.%, then disappear when the content of Al element is 3.0 wt.%. The size of $(Mg, Al)_3Gd$ phase increases with increasing the Al content, which changes from short fishbone-like in Mg-9Gd-0.4Al alloy to petal shaped in Mg-9Gd-1Al alloy. When the Al content increases further, the petal-like $(Mg, Al)_3Gd$ interconnect into a network. Fig. 1(d) and (e) presents the Al_2Gd phase appears and the size of particles increase with increasing of Al element.

The micrographs of solid solution treated (20 h) Mg-9Gd-xAl alloys are illustrated in Fig. 2. After solution treatment, the Mg_5Gd phase is hardly observed in all specimens. On the contrary, the morphology and size of Al_2Gd phase do not change during solid solution due to its high melt point [25]. Partial $(Mg, Al)_3Gd$ phases dissolve into Mg matrix but there are still

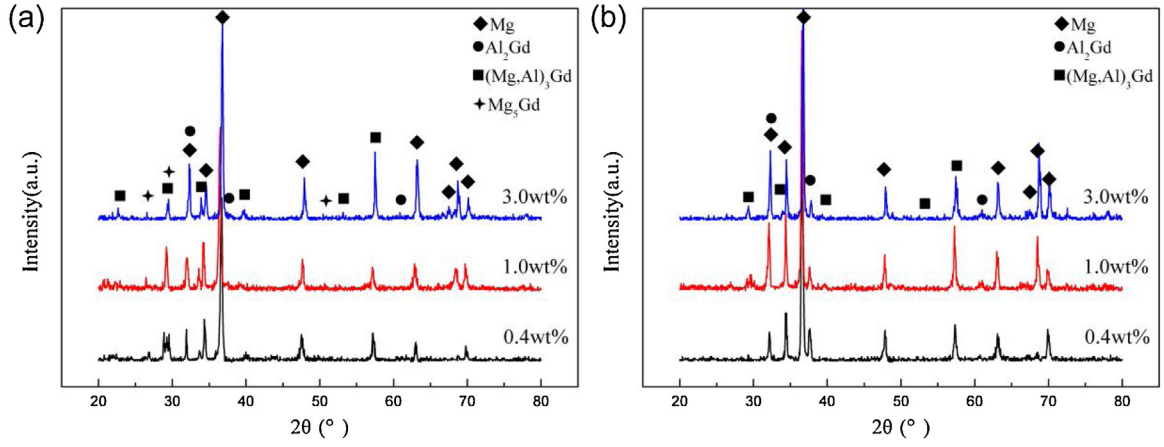

Fig. 4 – X-ray diffraction patterns of Mg-9Gd-xAl alloys under different states: (a) as-cast, (b) after solution treatment.

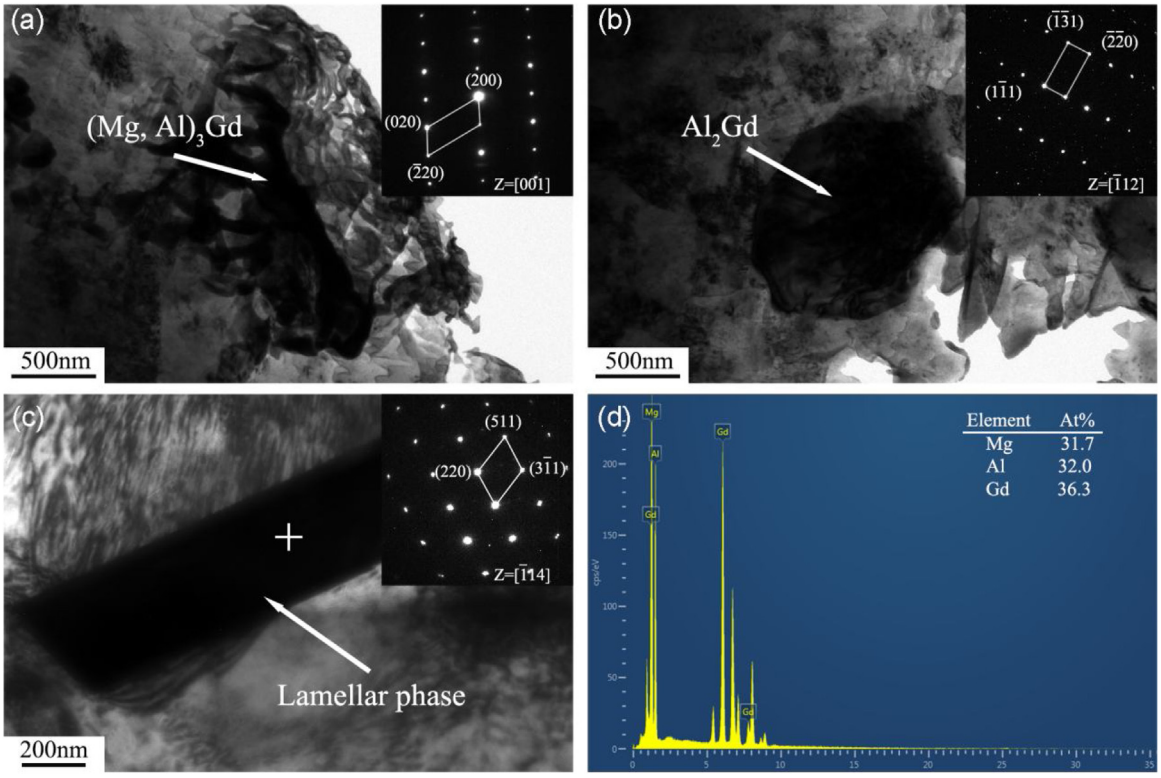

Fig. 5 – TEM morphology of different phases after different solution treatment by 20 h: (a) (Mg, Al)$_3$Gd phase, (b) Al$_2$Gd phase, (c) lamellar phase and the result of TEM-EDS (d).

some residual (Mg, Al)$_3$Gd and the amount of residue increases with increasing the Al content. In addition, it is interesting that there are a lot of lamellar phases formed in Mg-9Gd-xAl alloys ($x \leq 0.8$ wt.%) after solid solution treatment, which present parallel lamellar morphology within each grain and possess different parallel orientations in the adjacent grains. Besides, the lamellar precipitates sharply decrease with the Al content increased to 1.0 wt.%, and disappear when the Al content reaches 3 wt.%, illustrated in Fig. 2(e) and (f), respectively. The volume fraction and particle size of lamellar phase in Mg-9Gd-xAl alloys were statistically analyzed by ImageJ software. In order to minimize the statistical error, at least 10 SEM 3000* images were used, and then the statistical results should be averaged. The results were converted into a line chart as shown in Fig. 3. When the Al content belows 0.8 wt.%, the volume fraction of lamellar phase firstly increases and then decreases with the increasing Al content, but they are all above 10%. It is obviously that there is a sharp fall between 0.8 wt.% and 1.0 wt.%. The maximum value is 19.6% appearing in Mg-9Gd-0.6Al alloy. However, the size of lamellar phase has no obvious change with the Al content is less than 0.8 wt.%, which fluctuates in 2.29–2.44 μm, and decreases to 1.63 μm at 1.0 wt.% Al.

The X-ray diffraction patterns of as-cast and solid solution treated Mg-9Gd-xAl alloys ($x = 0.4$ wt.%, 1.0 wt.%, 3.0 wt.%) are exhibited in Fig. 4. It is obviously observed that the as-cast Mg-9Gd-xAl alloys consist by α-Mg, Al$_2$Gd, (Mg, Al)$_3$Gd and Mg$_5$Gd phase, which is consistent with the results of scanning observation. With increasing Al content from 0.4 to 3 wt.%, the intensity of the (Mg, Al)$_3$Gd phase at 23° and 57° increases, which indicates that the (Mg, Al)$_3$Gd phase increases with increasing the Al content [20,26]. By comparing the Fig. 4(a) with Fig. 4(b), the diffraction peaks of Mg$_5$Gd phase(PDFNo. 65-7133) disappear during the solid solution treatment. Moreover, the intensity of the Al$_2$Gd phase diffraction peaks at the degrees of about 32° and 37° increase [27]. However, it is surprising that no new crystallization peak appears in XRD pattern for parallel lamellar precipitates.

The crystal structure and composition of the lamellar phase were explored by TEM observation on the Mg-9Gd-0.6Al alloy. As shown in Fig. 5(a)–(c), the TEM morphology and SAED patterns of the second phase in the Mg-9Gd-0.6Al alloy have been given. Comparing Fig. 5(b) and (c), although the lamellar phase and the Al$_2$Gd phase under TEM have completely different morphology, the corresponding diffraction patterns specifically show that the crystal structure of lamellar phase is the same as the Al$_2$Gd ones (fcc) [23]. According to the calculation, the lattice parameter of the lamellar phase is 7.925 Å, which is close to that of Al$_2$Gd (7.903 Å, PDFNo. 65-5383). That is why there is no new diffraction peak in XRD measurement. The TEM-EDS results clearly show that the summation of the atomic percentage of Al and Mg is about twice that of Gd. Combined with the diffraction patterns and TEM-EDS results in Fig. 5(c) and (d), it is speculated that the lamellar phase is (Mg, Al)$_2$Gd phase.

In order to study the formation mechanism of the lamellar phase, Mg-9Gd-0.4Al alloy was selected for solution treatment. During the solution treatment, the lamellar phase increases

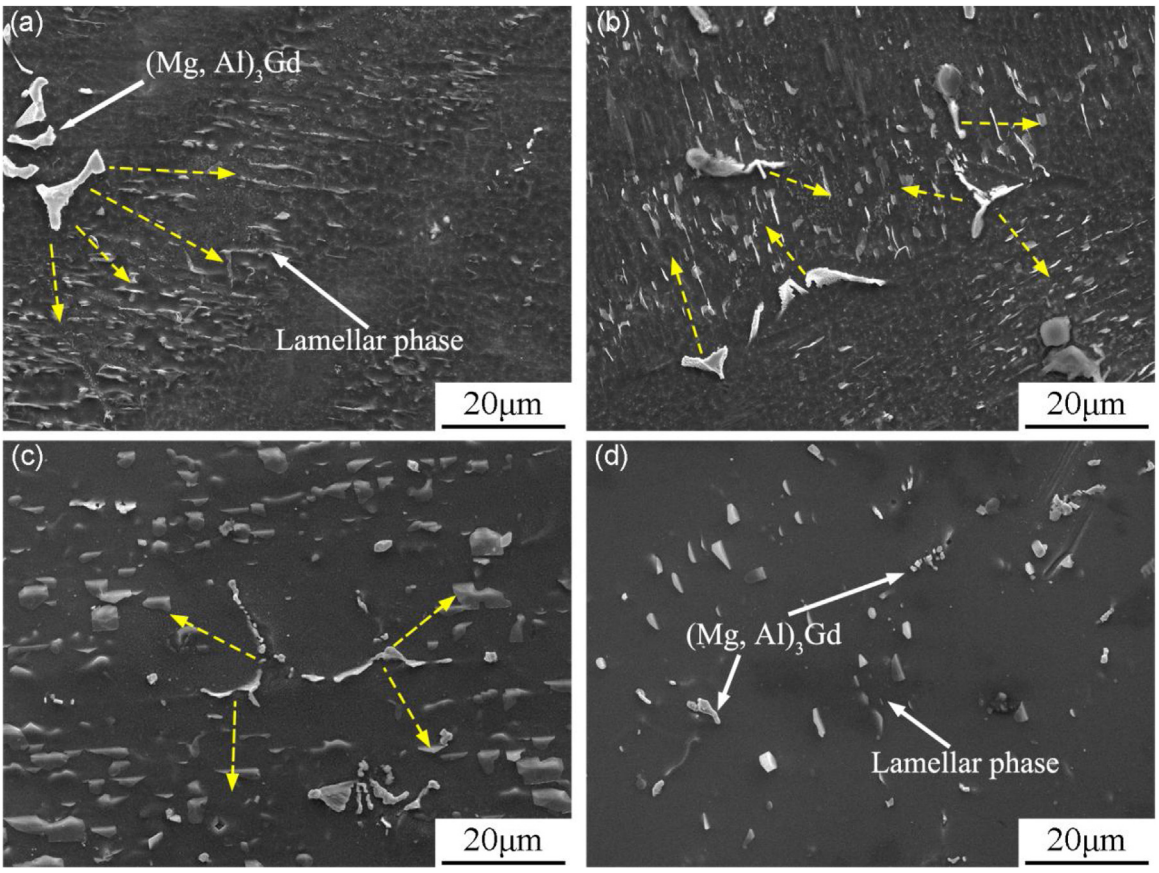

Fig. 6 – The SEM image of Mg-9Gd-0.4Al Alloy after different solution treatment time (a) 3 h, (b) 15 h, (c) 20 h, (d) 50 h.

while the $(Mg, Al)_3Gd$ phase and Mg_5Gd phase decrease in the Mg-9Gd-xAl alloys. Therefore, the formation of the lamellar phase is related to the consumption of $(Mg, Al)_3Gd$ phase and Mg_5Gd phase. As shown in Fig. 6, the yellow arrows in the figure indicate the diffusion paths of the Gd and Al elements. In the initial stage of solution treatment, the main elements, such as Gd and Al, begin to diffuse from the two second phases into the grain, meanwhile the Gd element in the Gd-rich regions also diffuse into the grain due to the atomic concentration difference [28]. Hence, inside the grain, the Gd element consists of two parts. One part is the Gd dissolved from the $(Mg, Al)_3Gd$, Mg_5Gd and Gd-rich region, the other is the original Gd in the α-Mg matrix, which makes the ratio of Gd to Al element in this region greater than 2. That is, the composition condition of the lamellar phase is satisfied in the region, so the initial line-like lamellar phase begins to appear. Nevertheless, there is no Gd enrichment region and Mg_5Gd in the as-cast Mg-9Gd-3Al alloy, as shown in Fig. 1. In addition, abundant Al_2Gd formed in the Mg-9Gd-3Al alloy consuming a lot of Gd elements, which is not dissolved into the matrix. Consequently, there is no sufficient Gd to meet the composition requirement, which results in no $(Mg, Al)_2Gd$ forming in solid solution treated Mg-9Gd-3Al alloy. As the solution treatment time increases, more Gd and Al elements diffuse into the region, and Mg, Gd, and Al elements continue to bond on one side of the lamellar phase improving the lamellar phase size. At the same time, the $(Mg, Al)_3Gd$ phase gradually disappears. When the solution treatment time continues to increase, both $(Mg, Al)_3Gd$ phase and lamellar phase dissolve in the matrix.

In order to further study the variation of lamellar phase with solid solution time, Mg-9Gd-0.6Al alloy was selected for solution treatment at smaller time intervals. The microstructures are shown in Fig. 7. The arrows in the figures indicate the directions of the lamellar phase, *l* indicates the length of the lamellar phase, and *b* indicates the width of the lamellar phase. The lamellar phase has not yet formed in the initial stage of the solution treatment, as shown in Fig. 7(a) and (b), which distributes inside the grain, and presents a short line shape. As the solution treatment time increases to 7.5 h, some linear lamellar phase grow into a rectangle shape and exhibit reproducible morphology. This indicates that there is a unique orientation relationship between the lamellar phase and the matrix, which is $(10\bar{1}0)_m \| (1\bar{1}00)_L$ (m represents the α-Mg matrix, L represents the lamellar phase)[23,29], as shown in Fig. 8. As the solution treatment time continues to increase to 20 h, all the linear lamellar phase almost changed into the rectangle lamellar and grew to thicker. When the solution treatment time reaches 35 h, the *b* of lamellar phase becomes larger while the *l* of lamellar phase does not change significantly. As the time extends to 50 h, the *b* of lamellar phase distributing in the matrix further decreases, as shown in Fig. 7(f), and some lamellar phases melt from the middle resulting in the smaller *l* of lamellar phase.

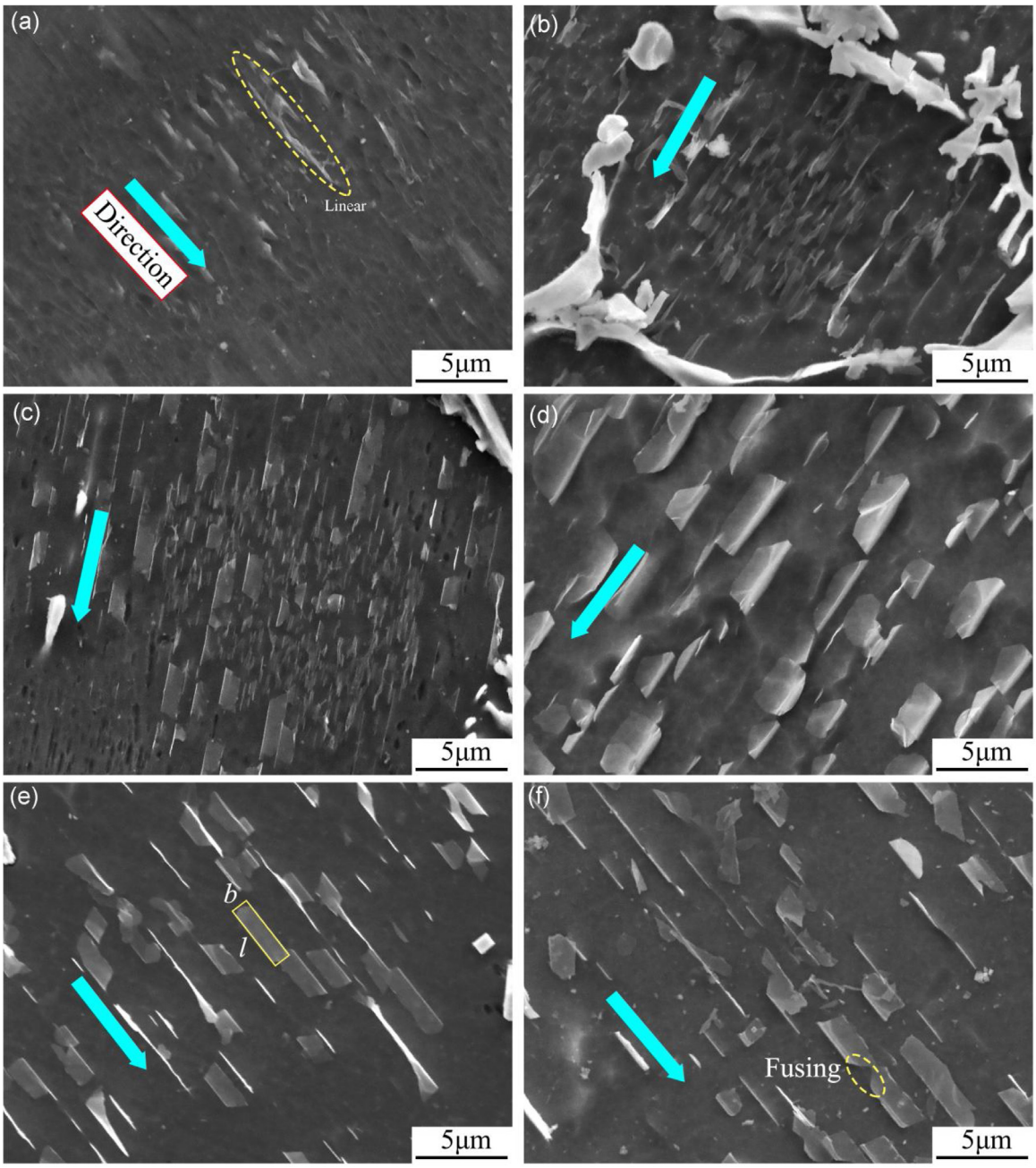

Fig. 7 – The lamellar phase in Mg-9Gd-0.6Al alloy at different solution time: (a) 1 h, (b) 3.5 h, (c) 7.5 h, (d) 20 h, (e) 35 h, (f) 50 h.

According to the above observation, the sketch map of lamellar phase morphology after solution treatment at different times can be shown in Fig. 9. The red arrows in the figure represent the diffusion direction. There is a large amount of $(Mg, Al)_3Gd$, Mg_5Gd and Gd element segregation zones along the grain boundary in the as-cast Mg-9Gd-xAl alloy. In the initial stage of solution treatment, the elements Gd and Al begin to diffuse into the matrix and the linear lamellar phase appears when the composition meets the requirements. When the solid solution treatment time is prolonged, the elements required for the lamellar phase assemble on one side of linear lamellar phase, resulting in the linear forms growing into rectangle. As the solution treatment time is prolonged to 20 h, the length of the lamellar phase is constant, the width is increased, and the particle size is maximized. When the solution treatment time continues to increase, the lamellar phase begins to dissolve into the matrix, and breaks at the intermediate position of the particles. Meanwhile, the elements in the lamellar phase diffuse toward the matrix, leading to a smaller width of lamellar phase, even partial lamellar phase dissolved in the matrix completely.

The Vickers hardness of Mg-9Gd-xAl at different solution treatment time is shown in Fig. 10. With the extension of the solution treatment time, the hardness of the alloy firstly decreases and then rises slightly in same composition, reach-

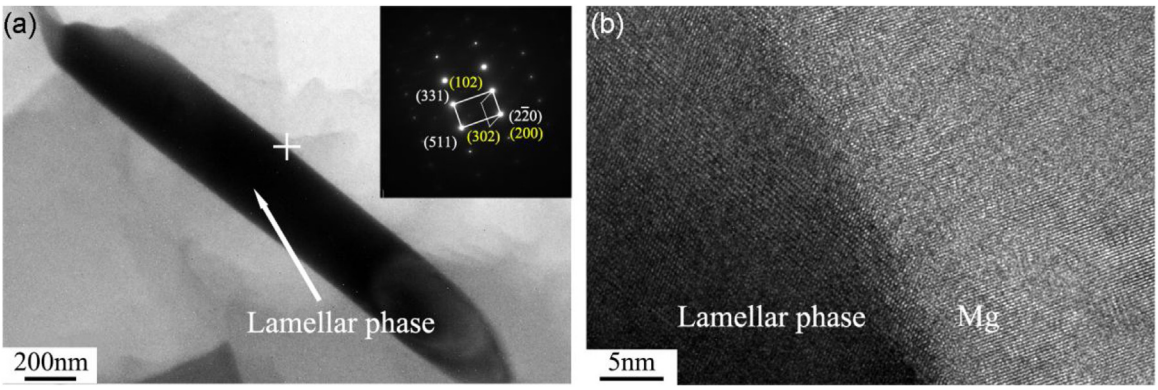

Fig. 8 – (a) TEM morphology of lamellar phase and corresponding diffraction pattern at the edge-on interface, yellow points belong to Mg, (b) HAADF-STEM image of the edge-on interface.

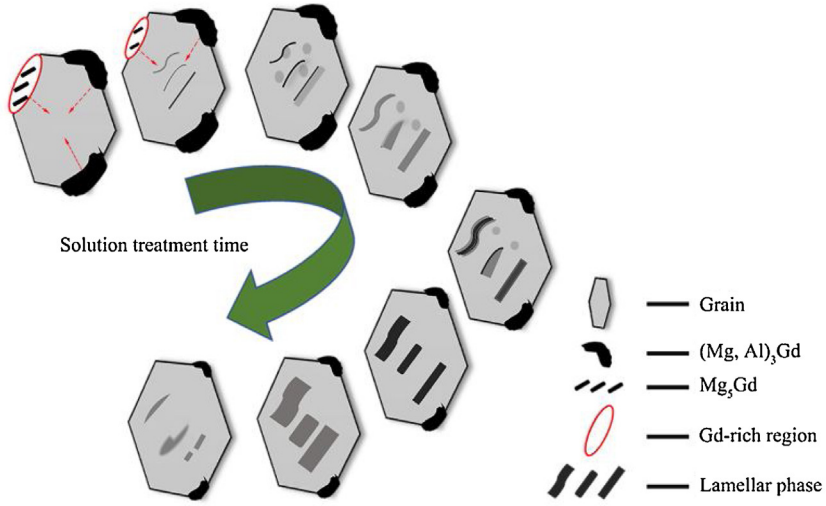

Fig. 9 – Lamellar phase formation diagram of Mg-9Gd-xAl alloy during solution treatment.

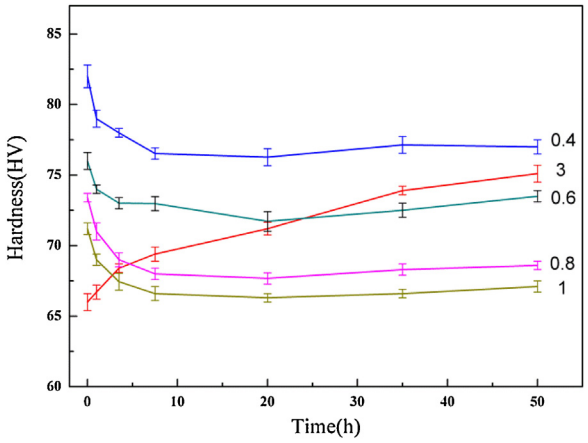

Fig. 10 – The hardness of Mg-9Gd-xAl at different solution treatment time (x = 0.4, 0.6, 0.8, 1.0, 3.0 wt. %).

ing the lowest value around 20 h. In addition, as the Al content increases, the Vickers hardness value of the alloy decreases.

In the initial stage of solution treatment, there are two main factors to reduce the hardness of the alloy. On the one hand, although according to the experimental principle of Vickers hardness [30–32], the dispersed lamellar phase will produce a distinct second phase strengthening, the large number of lamellar phases form inside the alloy grains consuming Gd and Al in the alloy, which results in a decrease in the solid solubility of the alloy matrix and a decrease in hardness. Jiwu et al. [33] found that the saturated solid solution fraction resolves the metal phase, causing the degree of supersaturation of the matrix to decrease, and resulting in a decrease in the hardness of the 7055 alloy. When the solution treatment time reaches about 20 h, as show in Fig. 4, the hardness of the alloy reaches the minimum value due to the maximum volume fraction of the lamellar phase precipitated inside the grain. On the other hand, the (Mg, Al)$_3$Gd phase and the Mg$_5$Gd phase are dissolved in the matrix during the solution treatment lead to a greatly reduced of volume fraction and size. Then, the strengthening effect from the two phases on the hardness in the alloy is weakened. The main factor to the improvement of hardness of the alloy is that both the (Mg, Al)$_3$Gd phase and the (Mg, Al)$_2$Gd phase are dissolved in the matrix as the solution treatment time increases, which will increase the matrix solid solution atoms and increase the lattice distortion. Therefore, the hardness of Mg-9Gd-xAl alloy increases when solution treatment for 20–50 h.

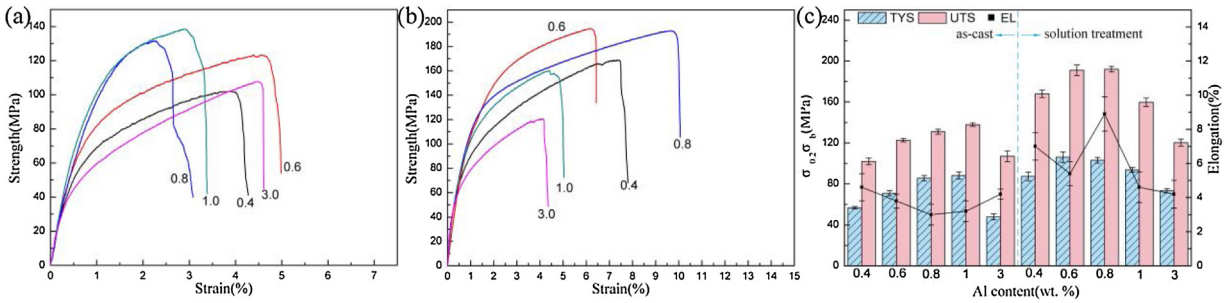

Fig. 11 – (a) Stress–strain curves of as-cast Mg-9Gd-xAl alloy, (b) stress–strain curves of Mg-9Gd-xAl alloy after solution treatment for 20 h and (c) the increase of ultimate tensile strength by solution treatment.

In addition, the atomic size difference between the Gd atoms and Mg atoms causes the production of lattice distortion in the α-Mg matrix resulting in the solid solution hardening [34,35]. Although the size of Al atoms is similar to Mg atoms, the added Al element weakens the lattice distortion caused by the Gd element. This leads to the smaller hardness value of the solid-solution state alloy in the larger of Al content.

While for the Mg-9Gd-3Al alloy, the hardness increases steadily with the time of solution treatment (Fig. 10), which is quite different from the other four alloys. This is because, in the Mg-9Gd-3Al alloy, there is no lamellar phase formed during the solution treatment, the solid solution atoms (Al, Gd) are dissolved into the matrix with the increase of time. Therefore, the hardness of the alloy is positively related to the solution time.

Fig. 11(a) and (b) are the stress-strain curves of the Mg-9Gd-xAl alloys before and after solution treatment. The solution treatment has a great influence on the Mg-9Gd-0.4Al, Mg-9Gd-0.6Al, and Mg-9Gd-0.8Al alloys as shown in Fig. 11(c). It is indicated that the Al element greatly improves the mechanical properties of the solid-solution state Mg-9Gd alloy. After solution treatment, the ultimate tensile strength of Mg-9Gd-0.6Al alloy is the highest, which is 57% higher than that of as-cast alloy. The increase value in ultimate tensile strength of Mg-9Gd-0.4Al alloy and Mg-9Gd-0.8Al alloy were 66 and 61 MPa, respectively.

The strengthening mechanisms of the solution-treated Mg-9Gd-xAl alloy mainly contains solid solution strengthening and second phase strengthening. Since the Al content is different, it is necessary to calculate the contribution value of solid solution strengthening after adding the Al element. According to the classical formula of solution strengthening, the contribution of solid solution strengthening is related to the 2/3 power of the solid solubility of Al in the alloy [36]. Therefore, in the Mg-9Gd-xAl alloy, the contribution of solid solution strengthening increases with the increase of Al content.

According to the principle of the second phase strengthening, the second phase distributed in the alloy greatly hinders the dislocation slip, and the effect is dictated to the size and volume fraction of the second phase. During the process of tensile deformation, the lamellar phase inside the grain can hinder the movement of dislocations to the grain boundary, so the dislocations are entangled near the lamellar phase particles. It results in the external force must be increased if the alloy continues to deform. Meanwhile, the $(Mg, Al)_3Gd$ phase is partially dissolved and becomes dispersed in the form of particles distributed near the grain boundary, which acts as a pinning grain boundary. Therefore, the strength of the alloy is significantly improved when the Al content is between 0.4 and 0.8 wt.%. Under the case of Al content more than 0.8 wt.%, only a little lamellar phase formed in the alloy, and the $(Mg, Al)_3Gd$ phase distributed at the grain boundary is still coarse after 20 h solution treatment. Consequently, the ultimate tensile strength of Mg-9Gd-1Al alloy and Mg-9Gd-3Al alloy increase less compared with the Mg-9Gd alloys with low Al content.

4. Conclusions

(1) The Mg_5Gd phase in the Mg-9Gd-xAl alloy disappears during solution treatment. As the solution treatment time increases, the fishbone or petal-like $(Mg, Al)_3Gd$ phase dissolves into the matrix, and the bulk Al_2Gd has almost no change. In addition, the lamellar phase is formed inside the crystal grains after the solution treatment.

(2) The lamellar phase in the Mg-9Gd alloy appears at a content of less than 1 wt.% of the Al element. As the solution treatment time increases, the lamellar phase eventually dissolves in the matrix. According to the diffraction patterns and TEM-EDS results, the lamellar phase can be determined as $(Mg, Al)_2Gd$ phase.

(3) After solution treatment of Mg-9Gd-xAl alloy, the lamellar phase inside the grain provides a strong second phase strengthening effect. The tensile strength of Mg-9Gd-0.6Al alloy is greatly improved, which is attributed to the combined action of solid solution strengthening and second phase strengthening.

Conflicts of interest

The authors declare that they have no known competing financial interests or personal relationships that could have appeared to influence the work reported in this paper.

Acknowledgments

This work was supported by National Natural Science Foundation of China (51704209, U1810208), Shanxi province

scientific facilities and instruments shared service platform of magnesium-based materials electric impulse aided forming (201805D141005), Science and Technology Major Project of Shanxi Province (20191102008, 20191102007, 20181101008), Natural Science Foundation of Shanxi Province (201701D121045), The Projects of International Cooperation in Shanxi (201803D421086) , Patent Implementation and Promotion Project of Shanxi Province (20200718).

REFERENCES

[1] Gan Wei, Liu Chenfu, Lu Fuqin, et al. Study on surface modification and properties of the AZ91D magnesium alloy used for automobile engine. J Mater Res Technol 2020, http://dx.doi.org/10.1016/j.jmrt.2020.03.084.
[2] Figueiredo RB, Langdon TG. Achieving superplastic properties in a ZK10 magnesium alloy processed by equal-channel angular pressing. J Mater Res Technol 2017;6(2):129–35.
[3] Cui Y, Li Y, Wang Z, Ding X, Koizumi Y, Bian H, et al. Impact of solute elements on detwinning in magnesium and its alloys. Int J Plast 2017;91:134–59.
[4] Lu L, Liu T, Chen Y, Wang Z. Deformation and fracture behavior of hot extruded Mg alloys AZ31. Mater Charact 2012;67:93–100.
[5] Yu H, Xin Y, Wang M, Liu Q. Hall–Petch relationship in Mg alloys: a review. J Mater Sci Technol 2018;34:248–56.
[6] Apps PJ, Karimzadeh H, King JF, Lorimer GW. Precipitation reactions in magnesium-rare earth alloys containing yttrium, gadolinium or dysprosium. Scr Mater 2003;48:1023–8.
[7] Bohlen J, Yi S, Letzig D, Kainer KU. Effect of rare earth elements on the microstructure and texture development in magnesium–manganese alloys during extrusion. Mater Sci Eng A 2010;527:7092–8.
[8] Mirzadeh H. Quantification of the strengthening effect of rare earth elements during hot deformation of Mg-Gd-Y-Zr magnesium alloy. J Mater Res Technol 2016;5(1): 1–4.
[9] Liu D, Yang D, Li X, Hu S. Mechanical properties, corrosion resistance and biocompatibilities of degradable Mg-RE alloys: a review. J Mater Res Technol 2019;8(1):1538–49.
[10] Huang H, Miao H, Yuan G, Chen C, Zhang H, Pei J. Deformation behavior and texture randomization of Mg–Zn–Gd alloys reinforced with icosahedral quasicrystal. Int J Mater Res 2017;108(6):455–64.
[11] Zhong L, Peng J, Sun S, Wang Y, Lu Y, Pan F. Microstructure and thermal conductivity of as-cast and as-solutionized Mg–rare earth binary alloys. J Mater Sci Technol 2017;33:1240–8.
[12] Nagarajan D. Anelasticity in cast Mg-Gd alloys. Mater Sci Eng A 2017;695:14–9.
[13] Xu Y, Gensch F, Ren Z, Kainer KU, Hort N. Effects of Gd solutes on hardness and yield strength of Mg alloys. Prog Nat Sci: Mater Int 2018;28:724–30.
[14] Fang C, Liu G, Liu X, Hao H, Zhang X. Significant texture weakening of Mg-8Gd-5Y-2Zn alloy by Al addition. Mater Sci Eng A 2017;701:314–8.
[15] Kishida K, Inoue A, Yokobayashia H, Inuia H. Deformation twinning in a Mg–Al–Gd ternary alloy containing precipitates with a long-period stacking-ordered (LPSO) structure. Scr Mater 2014;89:25–8.
[16] Pourbahari B, Mirzadeh H, Emamy M. Toward unraveling the effects of intermetallic compounds on the microstructure and mechanical properties of Mg–Gd–Al–Zn magnesium alloys in the as-cast, homogenized, and extruded conditions. Mater Sci Eng A 2017;680:39–46.
[17] Pourbahari B, Emamy M, Mirzadeh H. Synergistic effect of Al and Gd on enhancement of mechanical properties of magnesium alloys. Prog Nat Sci: Mater Int 2017;27(2): 228–35.
[18] Raghavan V. Al-Gd-Mg (aluminum-gadolinium-magnesium). J Phase Equilib Diffus 2007;28:464–8.
[19] Wang X, Du W, Liu K, Wang Z, Li S. Microstructure, tensile properties and creep behaviors of as-cast Mg–2Al–1Zn–xGd (x = 1, 2, 3, and 4 wt.%) alloys. J Alloys Compd 2012;522: 78–84.
[20] Dai J, Easton M, Zhu S, Wu G, Ding W. Grain refinement of Mg–10Gd alloy by Al additions. J Mater Res 2012;27(21):2790–7.
[21] Yokobayashi H, Kishida K, Inui H, Yamasaki M, Kawamura Y. Enrichment of Gd and Al atoms in the quadruple close packed planes and their in-plane long-range ordering in the long period stacking-ordered phase in the Mg–Al–Gd system. Acta Mater 2011;59(19):7287–99.
[22] Kishida K, Yokobayashi H, Inui H, Yamasaki M, Kawamura Y. The crystal structure of the LPSO phase of the 14 H-type in the Mg–Al–Gd alloy system. Intermetallics 2012;31(12): 55–64.
[23] Gu X-F, FuruharaGu T. Characterization of crystal structure and precipitation crystallography of a new $Mg_xAl_{2-x}Gd$ phase in an $Mg_{97}Al_1Gd_2$ alloy. J Appl Crystallogr 2016;49(4): 1177–81.
[24] Gu X. Near atomic row matching in the interface analyzed in both direct and reciprocal space. Crystals 2020;10(3): 192–208.
[25] Verbovytskyy Y, Gonçalves AP. On the ternary $RE_xMg_{1-x}Al_2$ (RE = Gd-Tm), $RE_3Ag_{5\pm x}Mg_{11\pm x}$, $REAg_{4+x}Mg_{2-x}$, $RE_4Ag_{10.3}Mg_{12}$ and $RE_4Ag_{10+x}Mg_{3-x}$ (RE = Ce-Nd, Sm) phases. Solid State Sci 2015;40: 84–91.
[26] Fang C, Liu G, Hao H, Wen Z, Zhang X. Effect of Al addition on microstructure, texture and mechanical properties of Mg-5Gd-2.5Y-2Zn alloy. J. Alloys Compd 2016;686: 347–55.
[27] Pourbahari B, Mirzadeh H, Emamy M. Elucidating the effect of intermetallic compounds on the behavior of Mg–Gd–Al–Zn magnesium alloys at elevated temperatures. J Mater Res 2017;32(22):4186–95.
[28] Huang H, Miao H, Yuan G, Chen C, Wang Z. Precipitation of secondary phase in Mg-Zn-Gd alloy after room-temperature deformation and annealing. J Mater Res Technol 2018;7(2):135–41.
[29] Fu GX, Zheng ZW. Application of the O-line model to martensite crystallography. Sci China: Technol Sci 2012;55(2):464–9.
[30] Guo B, Zhang L, Cao L, Zhang T, Jiang F, Yan L. The correction of temperature-dependent Vickers hardness of cemented carbide base on the developed high-temperature hardness tester. J Mater Process Technol 2018;255:426–33.
[31] Ozdogan A, Yesil ZD. Investigating the effect of different surface treatments on Vickers hardness and flexural strength of zirconium and lithium disilicate ceramics. J Prosthodontics 2020;29(2):129–35.
[32] Saboori Ah, Padovano E, Pavese M, Badini C. Novel magnesium elektron21-aln nanocomposites produced by ultrasound-assisted casting; microstructure, thermal and electrical conductivity. Materials 2018;11(1):27.
[33] Jiwu H, Zhimin Y, Jie L, Tao W. Effect of homogenization treatment on hardness and conductivity of 7055 alloy. Chin J Rare Met 2004;28(1):175–8.
[34] Janbozorgi M, Taheri KK, Taheri AK. Microstructural evolution, mechanical properties, and corrosion resistance

of a heat-treated Mg alloy for the bio-medical application. J Magnesium Alloys 2019;7(1):80–9.
[35] Bayat Tork N, Saghafian H, Razavi SH, Al-Fadhalah KJ, Ebrahimi R, Mahmudi R. Microstructure and texture characterization of Mg–Al and Mg–Gd binary alloys processed by simple shear extrusion. J Mater Res Technol 2019;8(1):1288–99.
[36] Toda-Caraballo I, Galindo-Nava EI, Rivera-Díaz-del-Castillo PEJ. Understanding the factors influencing yield strength on Mg alloys. Acta Mater 2014;75:287–96.